High-Performance of Electrocatalytic CO_2 Reduction on

Defective Graphene-Supported Cu_4S_2 Cluster

Qiyan Zhang[1], Yawei Li[1], Haiyan Zhu[1][*] and Bingbing Suo[1][*]

[1] Shaanxi Key Laboratory for Theoretical Physics Frontiers, Institute of Modern Physics, Northwest University, Xi'an 710127, China.

Corresponding author[*] Haiyan Zhu
Email: zhuhaiyan@nwu.edu.cn
Corresponding author[*] Bingbing Suo
Email: bsuo@nwu.edu.cn

Global minimum geometry composition research details

The global as well as local minima of cluster configurations for Cu_4X_2 and Cu_4X_4 clusters (X=O, S, Se) are searched by using the ABCluster structure prediction program based artificial bee colony algorithm [1-2]. The ABCluster global search technique employs potential energy function and mainly considers intermolecular Coulomb and Lennard-Jones interactions. In addition, the size of population of trial solution, the scout limit, and the maximum cycle number are required to be set to complete the geometry search [3-5]. The 500 disparate low-lying isomer structures can be generated from the above cluster searching process, and the top fifty low-lying structures are selected to be fully optimized at B3LYP/6-31g (d, p) level preliminarily. At this level, we choose the top 30% lower energy configurations to carry out the vibrational frequencies and Gibbs free energies calculations, and locate the global minima (GM) structure and low-lying energy isomers (ISO). Fig. S1 presents the GM structures of Cu_4X_2 (X=O, S, Se) as well as isomers within an energy window ranging from 0.674 up to 1.208 eV above the calculated GM energies. The geometric parameters and the maximum and minimum harmonic vibrational frequencies of the GM structure of the Cu_4X_2 cluster are listed in Table S1. Similarly, the global minima structures of Cu_4X_4 clusters are also determined via the same methods. In the following research, the global minima geometry composition of Cu_4X_2 and Cu_4X_4 as shown in Fig. S2 is leveraged as the most stable catalyst for the electrochemical CO_2 reduction process.
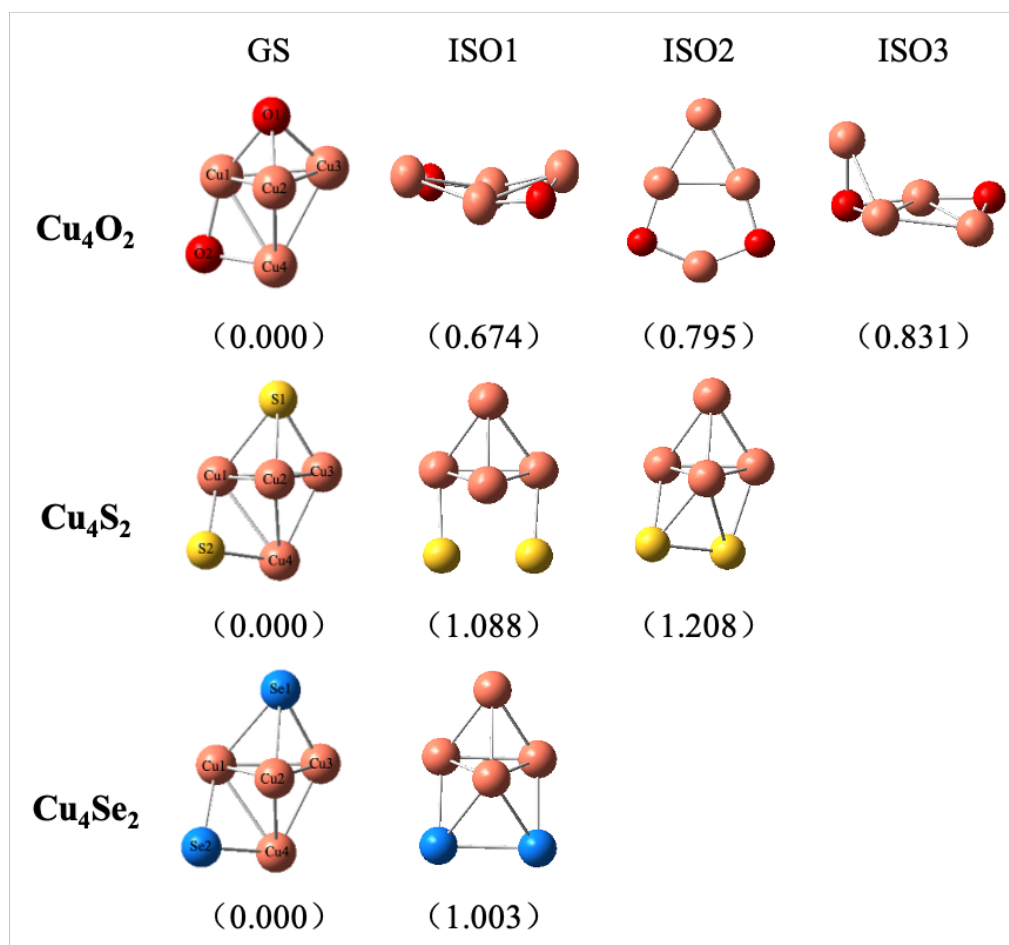
Figure S1. The ground minimal (GM) structures and low-lying energy isomers (ISO) of the gas-phase Cu_4X_2 clusters. The energy differences between the GM geometry and the corresponding isomers are presented by the parenthesis values in eV. (The orange, red, yellow and blue spheres are respectively describing the copper, oxygen, sulfur and selenium atom.)

For the Cu_4O_2 cluster, the stereoscopic structure of Cu_4 distorts significantly, giving rise to three low-lying energy configurations located +0.674, +0.795, and +0.831 eV above the GS structure. For the sulfur and selenium doped Cu_4X_2 cluster, the tetrahedral structure of Cu_4 is preserved in all optimized geometries, while the number of the Cu-X bonds is gradually decreasing in the high-energy isomer structures compared with the GM structure. Moreover, the electronegativity of Se is the weakest in three elements, thus Cu_4Se_2 has less isomers than the other two types of clusters.
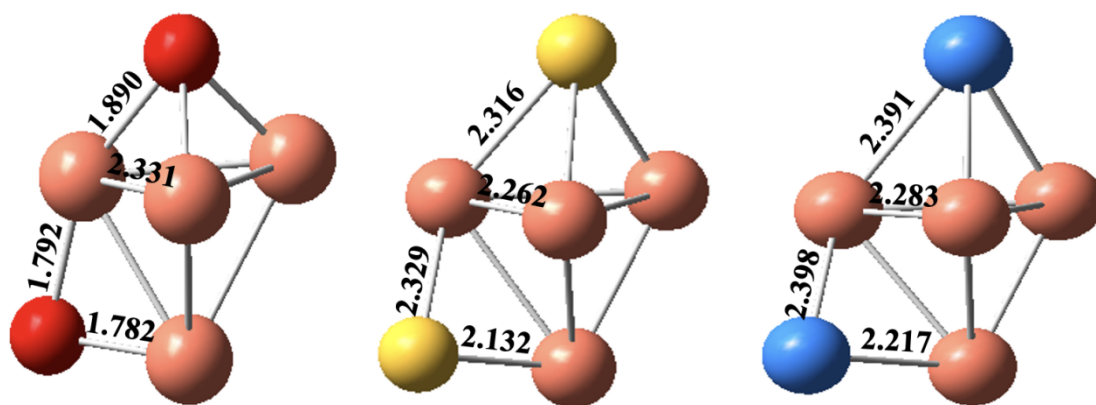
(a) Cu$_4$X$_2$ clusters
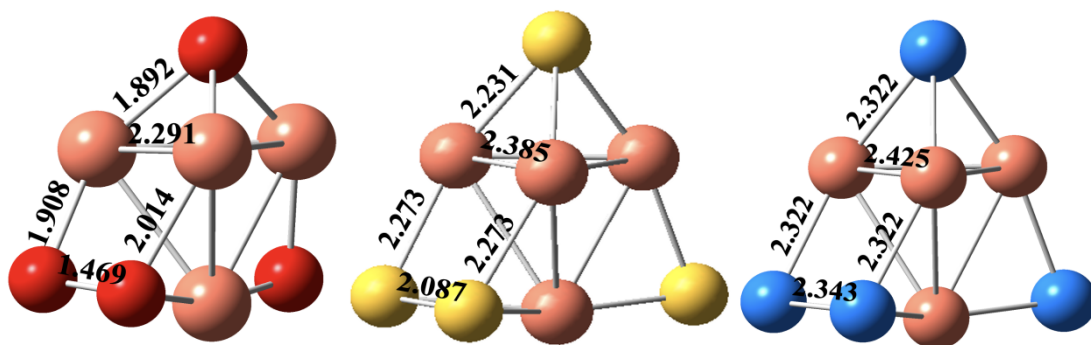
(b) Cu$_4$X$_4$ clusters

Figure S2. Global minimum geometry composition and some selected bond lengths (in Å) of Cu$_4$X$_2$ clusters (a) and Cu$_4$X$_4$ clusters (b). Red, yellow, blue, and orange spheres represent O, S, Se, and Cu atoms, respectively.

Table S1. Geometric parameters (in Å), the maximum, and minimum harmonic vibrational frequencies (in cm^{-1}) of the GM structure of gas-phase Cu_4X_2 clusters. $\bar{d}_{Cu_{xy}}$, $\bar{d}_{Cu_z}$, $\bar{d}_{(Cu-X_1)}$, and $\bar{d}_{(Cu-X_2)}$ refers to the averaged in-plane bond lengths of $Cu_{1,2,3}$ atoms, the averaged vertical-axis bond lengths between $Cu_{1,2,3}$ and Cu_4 atom, the averaged bond lengths between $Cu_{1,2,3}$ and doped X_1 atom, and the averaged bond lengths between $Cu_{1,4}$ and doped X_2 atom.

cluster	$\bar{d}_{Cu_{xy}}$	$\bar{d}_{Cu_z}$	$\bar{d}_{(Cu-X_1)}$	$\bar{d}_{(Cu-X_2)}$	ω_{max}	ω_{max}
Cu_4O_2	2.340	2.486	1.873	1.787	690.28	52.45
Cu_4S_2	2.387	2.445	2.259	2.230	411.83	14.51
Cu_4Se_2	2.419	2.448	2.335	2.308	329.46	15.21

As can be seen in Table S1, $\bar{d}_{Cu_{xy}}$, $\bar{d}_{(Cu-X_1)}$, and $\bar{d}_{(Cu-X_2)}$ increase linearly with the decrease of electronegativity of the doped atom in the GM structure, while $\bar{d}_{Cu_z}$ decreases about 0.04 Å from Cu_4O_2 to Cu_4S_2 and Cu_4Se_2. In addition, the positive vibrational frequencies (ω) indicated that the Cu_4X_2 geometries are local minima at the PES and have no transition state.

Table S2. The charge distribution of elements in the neutral Cu_4X, Cu_4X_2, and Cu_4X_4 clusters by the natural bond orbital (NBO) charge (e) analysis.

| Cluster	Atom	NBO	Cluster	Atom	NBO	Cluster	Atom	NBO
Cu_4O [a]	Cu1	0.474	Cu_4S [a]	Cu1	0.373	Cu_4Se [a]	Cu1	0.323
	Cu2	0.475		Cu2	0.373		Cu2	0.323
	Cu3	0.475		Cu3	0.373		Cu3	0.323
	Cu4	-0.160		Cu4	-0.013		Cu4	0.002
	O1	-1.264		S1	-1.105		Se1	-0.971
Cu_4O_2	Cu1	0.469	Cu_4S_2	Cu1	0.429	Cu_4Se_2	Cu1	0.343
	Cu2	0.625		Cu2	0.429		Cu2	0.343
	Cu3	0.625		Cu3	0.551		Cu3	0.509
	Cu4	0.551		Cu4	0.550		Cu4	0.509
	O1	-1.185		S1	-0.979		Se1	-0.852
	O2	-1.085		S2	-0.979		Se2	-0.852
Cu_4O_4	Cu1	0.765	Cu_4S_4	Cu1	0.518	Cu_4Se_4	Cu1	0.423
	Cu2	0.779		Cu2	0.518		Cu2	0.423
	Cu3	0.827		Cu3	0.423		Cu3	0.347
	Cu4	0.863		Cu4	0.407		Cu4	0.283
	O1	-1.121		S1	-0.882		Se1	-0.768
	O2	-0.567		S2	-0.241		Se2	-0.170
	O3	-0.605		S3	-0.241		Se3	-0.170
	O4	-0.941		S4	-0.504		Se4	0.369

[a] Reference [6]

Table S3. The charge distribution of elements in the neutral Cu_4X, Cu_4X_2, and Cu_4X_4 clusters with electrochemical CO_2 adsorption by the natural bond orbital (NBO) charge (e) analysis. The O^1 and O^2 represent the two oxygen atoms of COOH*.

Cluster	Atom	NBO	Cluster	Atom	NBO	Cluster	Atom	NBO
Cu_4O [a]	Cu1	0.537	Cu_4S [a]	Cu1	0.428	Cu_4Se [a]	Cu1	0.384
	Cu2	0.536		Cu2	0.428		Cu2	0.384
	Cu3	0.466		Cu3	0.339		Cu3	0.302
	Cu4	0.223		Cu4	0.337		Cu4	0.347
	O1	-1.187		S1	-0.975		Se1	-0.861
	C	0.421		C	0.432		C	0.431
	O^1	-0.721		O^1	-0.719		O^1	-0.719
	O^2	-0.770		O^2	-0.768		O^2	-0.768
	H	0.496		H	0.499		H	0.499
Cu_4O_2	Cu1	0.898	Cu_4S_2	Cu1	0.619	Cu_4Se_2	Cu1	0.460
	Cu2	0.898		Cu2	0.618		Cu2	0.638
	Cu3	0.448		Cu3	0.410		Cu3	0.381
	Cu4	0.604		Cu4	0.543		Cu4	0.521
	O1	-1.145		S1	-0.833		Se1	-0.735
	O2	-1.152		S2	-0.841		Se2	-0.747
	C	0.429		C	0.445		C	0.444
	O^1	-0.716		O^1	-0.713		O^1	-0.714
	O^2	-0.765		O^2	-0.751		O^2	-0.752
	H	0.498		H	0.503		H	0.503
Cu_4O_4	Cu1	1.086	Cu_4S_4	Cu1	0.845	Cu_4Se_4	Cu1	0.482
	Cu2	0.844		Cu2	0.606		Cu2	0.627
	Cu3	1.238		Cu3	1.015		Cu3	0.917
	Cu4	1.186		Cu4	0.809		Cu4	0.747
	O1	-1.215		S1	-0.908		Se1	-0.758

O2	-0.647		S2	-0.408		Se2	-0.342
O3	-0.645		S3	-0.422		Se3	-0.284
O4	-1.203		S4	-0.942		Se4	-0.762
C	0.715		C	0.723		C	0.709
O^1	-0.759		O^1	-0.753		O^1	-0.790
O^2	-0.781		O^2	-0.760		O^2	-0.726
H	0.181		H	0.193		H	0.179

[a] Reference [6]

Feasible reaction pathways of CO₂RR to methanol or methane on Cu₄X₂ cluster
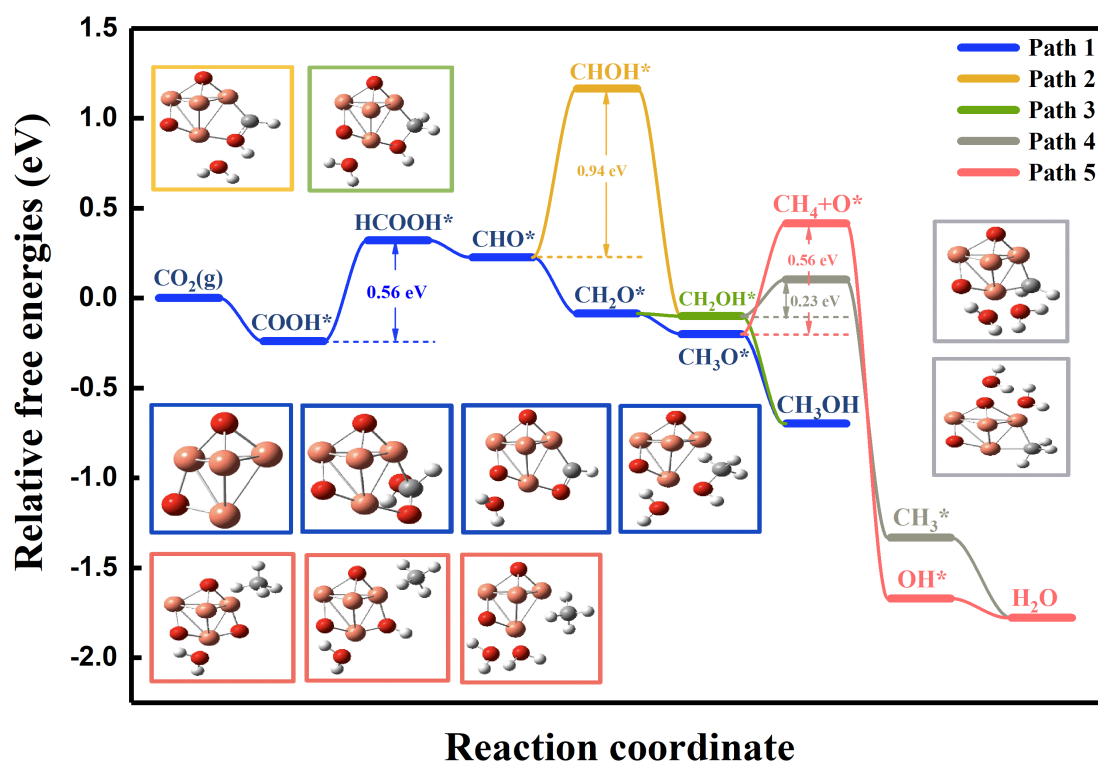
(a)
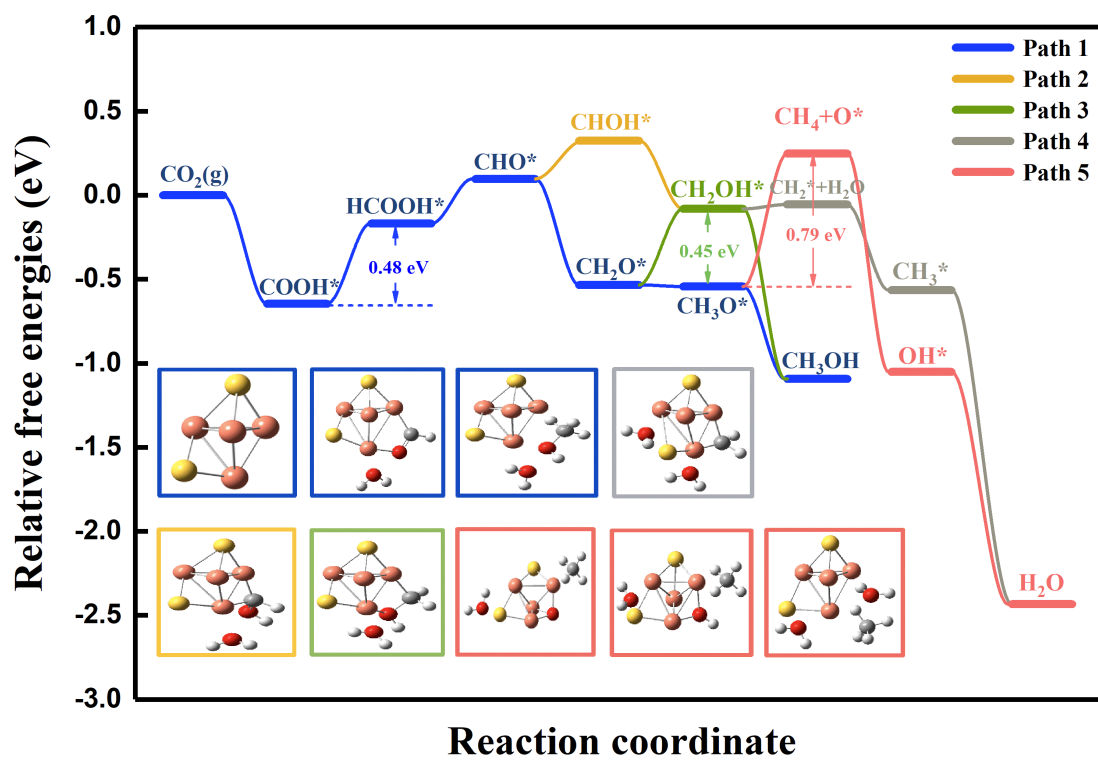
(b)
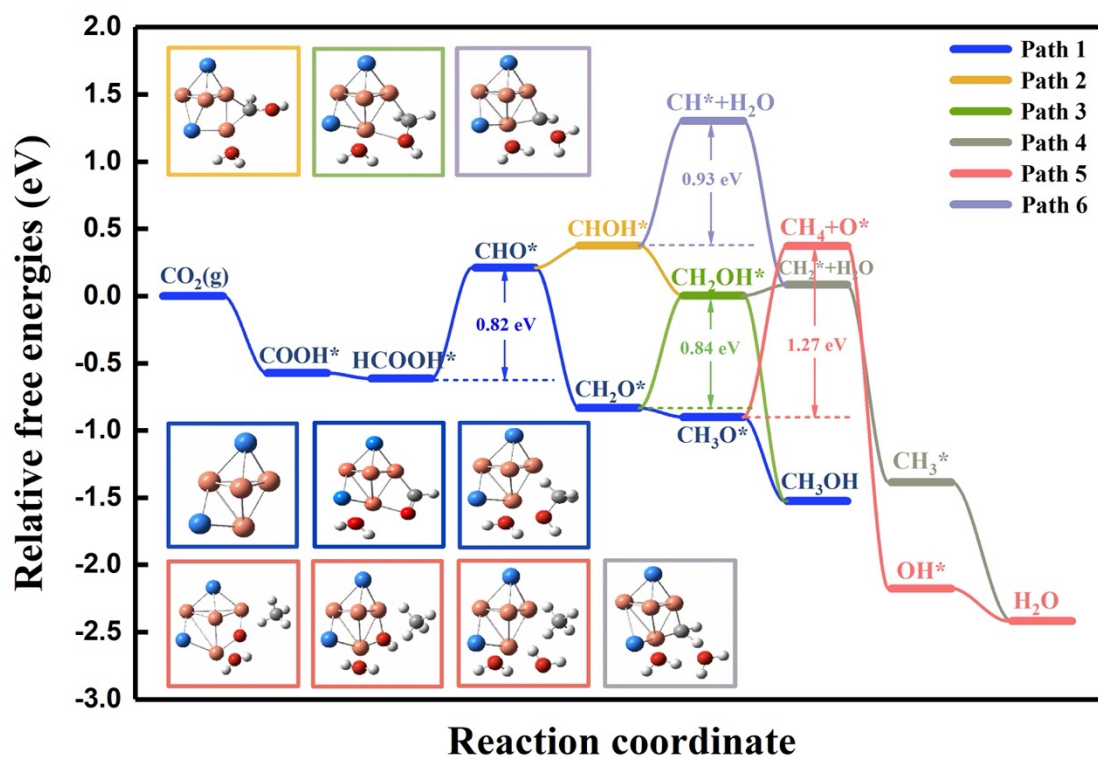
(c)

Figure S3. Mechanistic free energies diagram of electrochemical CO_2 reduction on Cu_4O_2 cluster (a), Cu_4S_2 cluster (b), and Cu_4Se_2 cluster (c) with no applied potential. The colorful lines are labeled thermodynamically feasible reaction pathways of CO_2RR towards methanol and methane. The optimized cluster structures of selected intermediates and final products are shown in insets. Red, yellow, blue, orange, grey, and white spheres represent O, S, Se, Cu, C, and H atoms, respectively.

Competitive reactions of Cu$_4$X$_2$ cluster
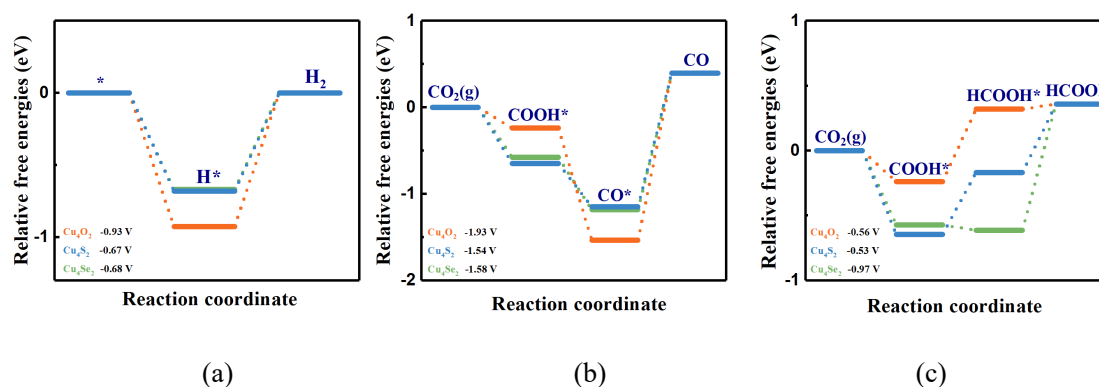
Figure S4. Free energies diagram for producing H$_2$ (a), CO (b), and HCOOH (c) with no applied potential. The orange, blue, and green lines represent Cu$_4$O$_2$, Cu$_4$S$_2$, and Cu$_4$Se$_2$ cluster, respectively. The potentials required to carry out over the most endergonic step are listed in the legend.

Among the pathway of CH$_3$OH and CH$_4$ formation, there are other competing reaction pathways that generate H$_2$, CO, and HCOOH. They exhibit significant differences in the efficiency and selectivity of CO$_2$ reduction to different products. Fig. S4(a) shows the pathways for the hydrogen evolution reaction (HER) on these three clusters. The Cu$_4$S$_2$ and Cu$_4$Se$_2$ cluster has small limiting potentials of -0.67 and -0.68 V, respectively, while the Cu$_4$O$_2$ cluster displays a slightly higher limiting potential of -0.93 V for HER. The CO$_2$ reduction pathway can also produce CO (in Fig. S4(b)) and HCOOH (in Fig. S4(c)). The CO release follows by the path CO$_2$→COOH*→CO*→ CO, and HCOOH is produced by the formation of HCOOH*. For the CO formation, the step of CO desorption from the cluster corresponds to the rate-determining step with reaction free energy all above 1.5 eV, which indicates that the amount of CO formation in these catalysts is low. The production of HCOOH follows a different trend than the other side reactions. Cu$_4$O$_2$ and Cu$_4$S$_2$ clusters exhibit the limiting potential of about -0.55 V, while the Cu$_4$Se$_2$ cluster has the most negative limiting potential of -0.97 V. It is noteworthy that although the rate-determining step of HCOOH, CH$_3$OH, and CH$_4$ production on the Cu$_4$O$_2$ cluster is all the COOH*→ HCOOH*, the formation of HCOOH requires an endothermic reaction, whereas the other two paths follow a downhill trend to achieve a more favorable occurrence. Generally speaking, the reactivity order of hydrocarbons production from the CO$_2$RR on the Cu$_4$X$_2$ cluster is in the order CH$_3$OH > CH$_4$ > HCOOH > CO.

Kinetic barrier diagram of key step on Cu_4X_2 cluster
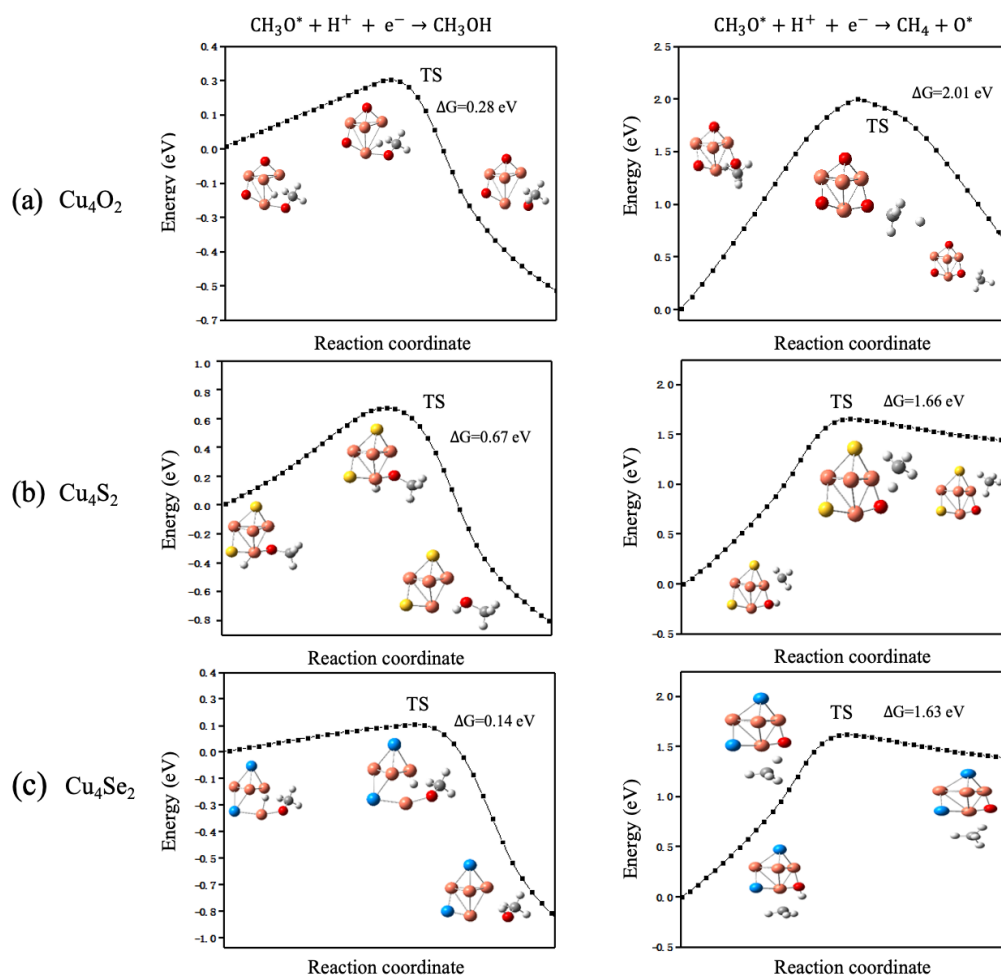

Figure S5. Kinetic barrier diagram of product-determining step on Cu_4O_2 cluster (a), Cu_4S_2 cluster (b), Cu_4Se_2 cluster (c). The figure on the left represents the step of $CH_3O^* + H^+ + e^- \rightarrow CH_3OH$, and the figure on the right represents the step of $CH_3O^* + H^+ + e^- \rightarrow CH_4 + O^*$. The energy barrier is listed in the legend. Red, yellow, blue, and orange spheres represent O, S, Se, and Cu atoms, respectively.

**Feasible reaction pathways of CO$_2$RR on Cu$_4$X$_4$ cluster**
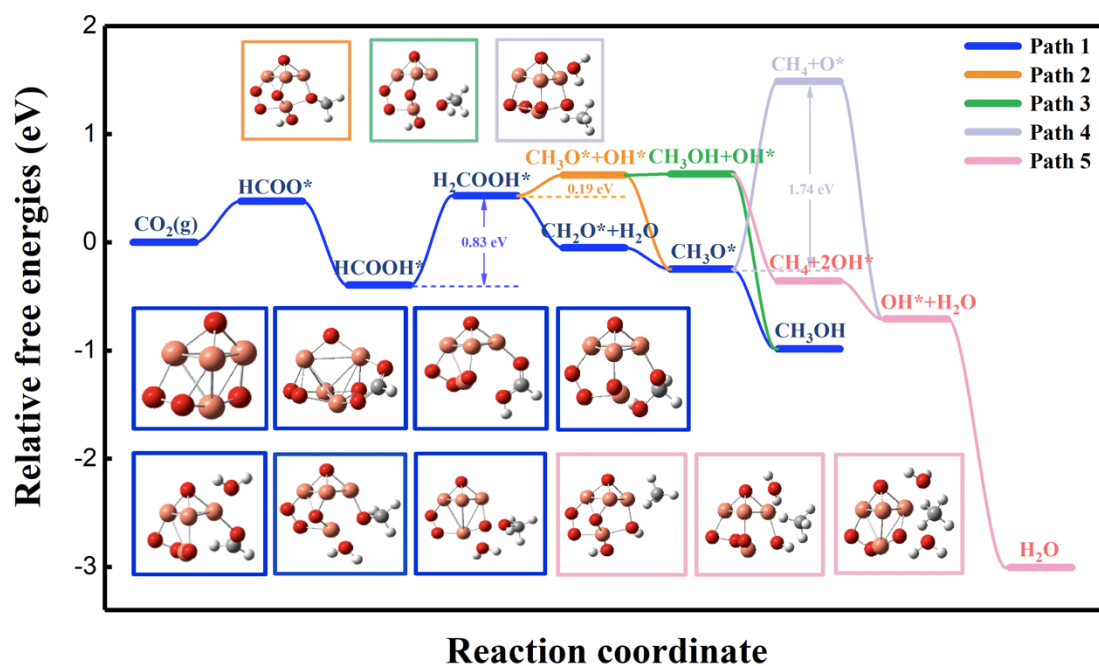
(a)
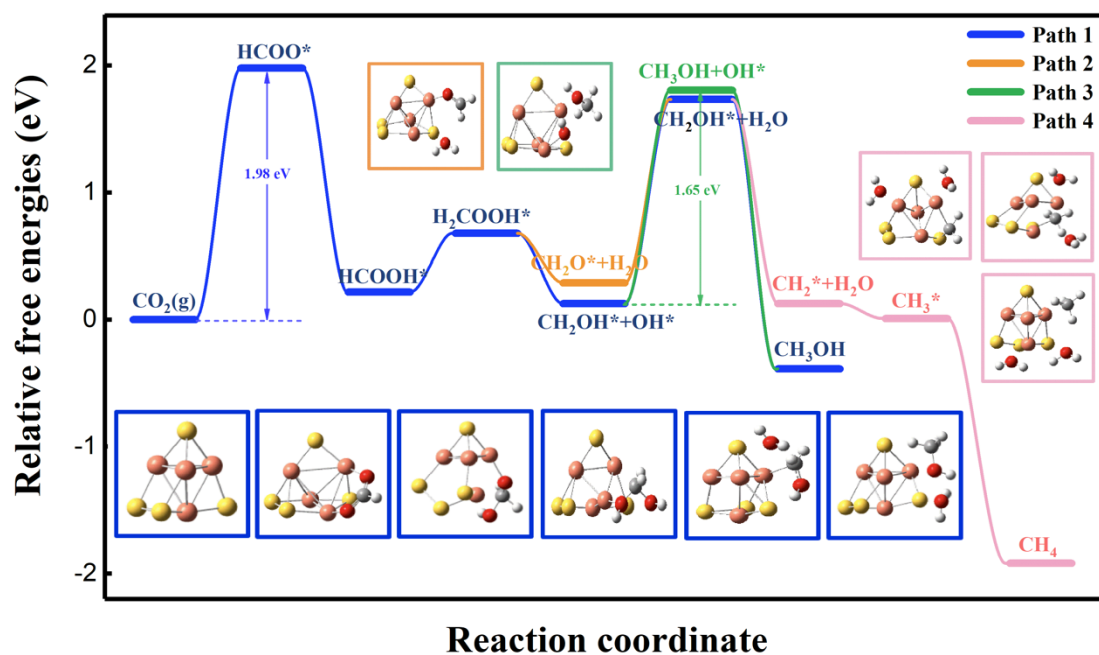
(b)
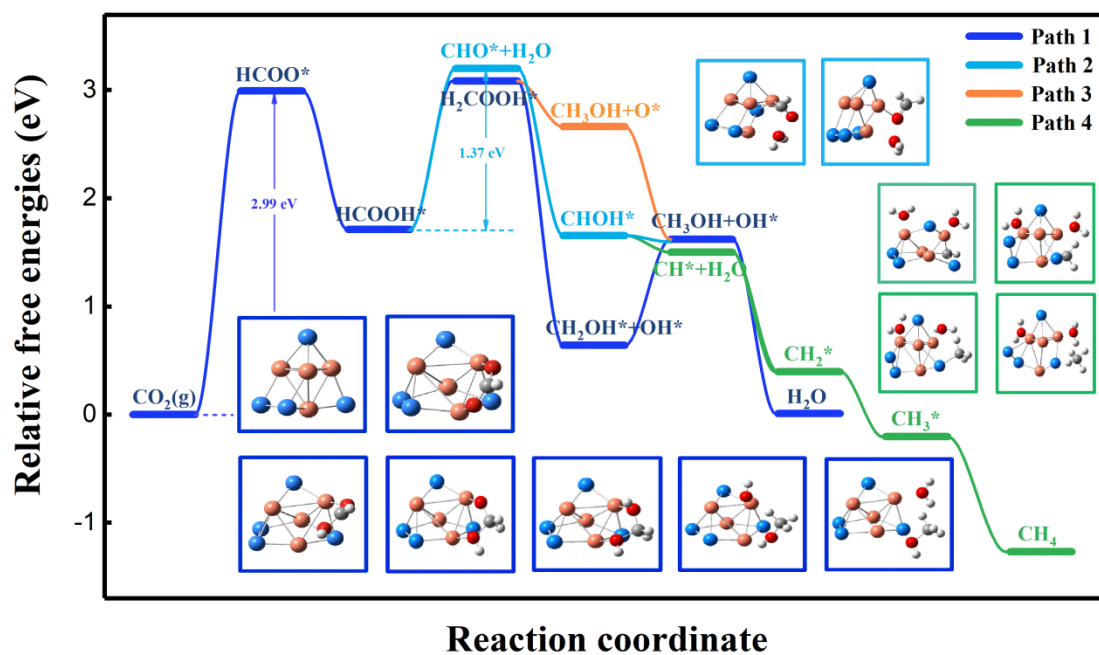
(c)

Figure S6. Mechanistic free energies diagram of electrochemical CO_2 reduction on the (a) Cu_4O_4 cluster, (b) Cu_4S_4 cluster, and (c) Cu_4Se_4 cluster with no applied potential. The colorful lines are labeled thermodynamically feasible reaction pathways of CO_2RR on Cu_4X_4 cluster. The optimized cluster structures of selected intermediates and final products are shown in insets. Red, yellow, blue, orange, grey, and white spheres represent O, S, Se, Cu, C, and H atoms, respectively.

As shown in Fig. S5, the CO_2 activation is more likely to occur on the C atom for the Cu_4X_4 cluster, which is the key point that leads to the hydrocarbon pathway follows completely different from that on the Cu_4X_2 clusters. In the CO_2RR pathway on the Cu_4O_4 cluster, the rate-determining step is the hydrogenation of HCOOH* with a limiting potential of -0.83 V. For the Cu_4S_4 and Cu_4Se_4 cluster, it is found that the pathway through HCOO* is not theoretically feasible, due to the reason that the free energy changes of the first protonation step is really high with no applied voltage.
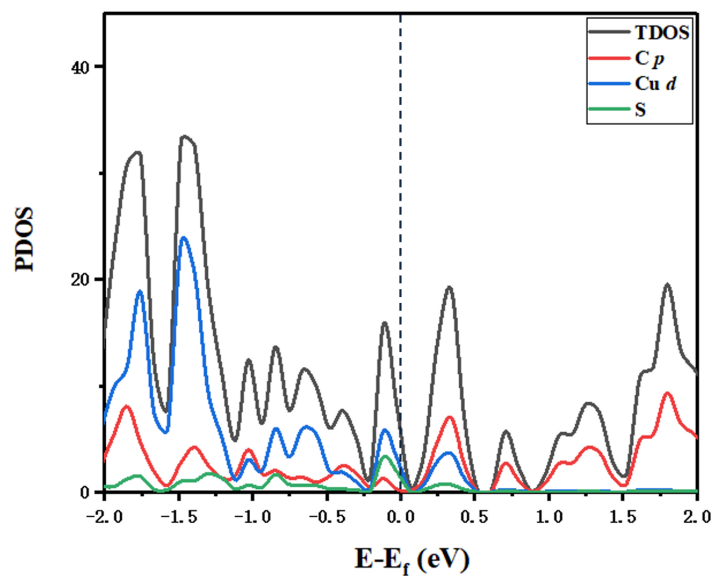
Figure S7. Total density of states (DOS) of Cu_4S_2/SV catalyst, Projected density of states (PDOS) of p orbitals of C, and PDOS of d orbitals of Cu. The dash line represents Fermi-level.
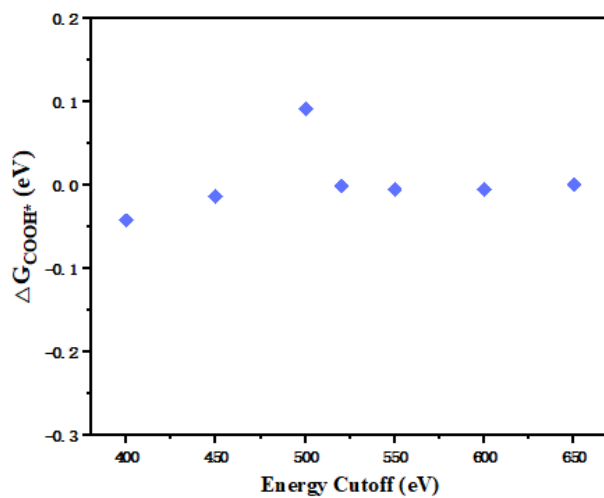

Figure S8. Variation the reaction free energy of COOH* on Cu_4S_2/SV catalyst as a function of the cutoff energy value in the plane-wave calculations. The calculated results at a cutoff of 520 eV is set to reference zero for easy comparison.

References

[1] Zhang, J., et al. "NWPEsSe: an Adaptive-Learning Global Optimization Algorithm for Nanosized Cluster Systems." Journal of Chemical Theory and Computation (2020).

[2] Malloum, A., J. J. Fifen, and J. Conradie. "Exploration of the potential energy surface of the ethanol hexamer." The Journal of Chemical Physics 150.12(2019).

[3] Khan, A. M., et al. "Analysis and assessment of the structural, electronic properties of $(ZrH_2)_n$ (n=5-24) clusters: Density function theory calculations." Computational and Theoretical Chemistry 1188(2020):112940.

[4] Ama, B, and JC A. "Solvent effects on the structures of the neutral ammonia clusters." Computational and Theoretical Chemistry 1191(2020).

[5] Malloum, A., JJ Fifen, and J Conradie. "Large-Sized Ammonia Clusters and Solvation Energies of the Proton in Ammonia." Journal of Computational Chemistry (2020).

[6] Zhang, Q.Y., Zhao Q.F., Zhu, H.Y., Suo B.B., et al. "Computational studies of electrochemical CO_2 reduction on chalcogen doped Cu_4 cluster." International Journal of Hydrogen Energy 43(2018).